Inorg. Chem. **2005**, *44*, 306–315

Cooperative Pull and Push Effects on the O–O Bond Cleavage in Acylperoxo Complexes of [(Salen)Mn^{III}L]: Ensuring Formation of Manganese(V) Oxo Species

Ilja V. Khavrutskii,† Djamaladdin G. Musaev,* and Keiji Morokuma*

Cherry L. Emerson Center for Scientific Computation and Department of Chemistry, Emory University, Atlanta, Georgia 30322

Received July 22, 2004

The acidity (pull) and the axial ligand (push) effects on the O–O bond cleavage in the [(Salen)Mn^{III}(RCO_3)L] acylperoxo complexes, with model L = none, NH_3, and HCO_2^- (**1**), have been studied with B3LYP density functional calculations. The acidic conditions have been mimicked by explicit protonation of **1** to afford a variety of [(Salen)Mn^{III}(RCO_3H)L] (**2**) and [(SalenH)Mn^{III}(RCO_3)L] (**3**) complexes in ground quintet states. The protonation assists the O–O bond heterolysis, thus primarily forming highly reactive Mn^{V}(O) species, and consequently suppresses formation of the less reactive Mn^{IV}(O) species through homolytic channel described earlier in **1** [Khavrutskii, I. V.; Rahim, R. R.; Musaev, D. G.; Morokuma, K. *J. Phys. Chem. B* **2004**, *108*, 3845–3854]. In addition to the qualitative change of the O–O bond cleavage mode, the protonation affects the rate of the O–O bond cleavage. Therefore, varying the acidity of the reaction media helps control the O–O bond cleavage mode and rate.

I. Introduction

Transition-metal-catalyzed enantioselective monooxygenation of organic substrates is one of the major challenges in synthetic and biological inorganic chemistry.[1−7] A number of transition-metal-containing enzymes and synthetic systems activate the O−X bond of various oxidants followed by the oxygen atom transfer to the substrate molecule in enantioselective fashion.[1,2] The key step of these processes is the heterolysis of the O−X bond leading to the highly reactive high-valent metal oxo species (such as formally Fe^{V}(O), Mn^{V}(O), etc.).[1,6,8,9] Homolysis of the O−X bond produces much less reactive oxo species (such as Fe^{IV}(O), Mn^{IV}(O), etc.) and hazardous free radicals and, therefore, must be avoided. The best enzymes for enantioselective monooxygenation, namely heme-containing peroxidases and P-450 cytochromes,[6,8,9] ensure heterolysis of the O−X bond through sophisticated machinery of special active site residues.[9−13]

* To whom correspondence should be addressed. E-mail: dmusaev@emory.edu (D.G.M.), morokuma@emory.edu (K.M.).

† Current address: Department of Molecular Biology, The Scripps Research Institute, La Jolla, CA 92037.

(1) Allain, E. J.; Hager, L. P.; Deng, L.; Jacobsen, E. N. *J. Am. Chem. Soc.* **1993**, *115*, 4415−4416.

(2) Jacobsen, E. N. In *Catalytic Asymmetric Synthesis*, 1st ed.; Ojima, I., Ed.; VCH Publishers: New York, 1993; pp 159−202.

(3) Jacobsen, E. N.; Wu, M. H. In *Comprehensive Asymmetric Catalysis: Asymmetric Synthesis and Induction Catalysts*; Jacobsen, E. N., Pfaltz, A., Yamamoto, H., Eds.; Springer: Berlin, New York, 1999; Vol. 2, pp 649−677. Katsuki, T. *J. Mol. Catal. A: Chem.* **1996**, *113*, 87−107. Katsuki, T. In *Catalytic Asymmetric Synthesis*, 2nd ed.; Ojima, I., Ed.; Wiley-VCH: New York, 2000; pp 287−325. Katsuki, T. *Curr. Org. Chem.* **2001**, *5*, 663−678. Katsuki, T. *Adv. Synth. Catal.* **2002**, *344*, 131−147.

(4) Palucki, M.; Pospisil, P. J.; Zhang, W.; Jacobsen, E. N. *J. Am. Chem. Soc.* **1994**, *116*, 9333−9334. Palucki, M.; McCormick, G. J.; Jacobsen, E. N. *Tetrahedron Lett.* **1995**, *36*, 5457−5460.

(5) Katsuki, T. *Coord. Chem. Rev.* **1995**, *140*, 189−214.

(6) Rantwijk, F.; Sheldon, R. A. *Curr. Opin. Biotechnol.* **2000**, *11*, 554−564. Velde, F.; Rantwijk, F.; Sheldon, R. A. *J. Mol. Catal. B: Enzym.* **1999**, *6*, 453−461. Velde, F.; Bakker, M.; Rantwijk, F.; Sheldon, R. A. *Biotechnol. Bioeng.* **2001**, *72*, 523−529. Velde, F.; Rantwijk, F.; Sheldon, R. A. *Trends Biotechnol.* **2001**, *19*, 73−79.

(7) Velde, F.; Konemann, L.; Rantwijk, F.; Sheldon, R. A. *Biotechnol. Bioeng.* **2000**, *67*, 87−96.

(8) Archelas, A.; Furstoss, R. In *Biocatalysis-From Discovery to Application*; Fessner, W.-D., Ed.; Springer: New York, 1999; Vol. 200, pp 159−191. Martinez, C. A.; Stewart, J. D. *Curr. Org. Chem.* **2000**, *4*, 263−282. Hu, S.; Hager, L. P. *Tetrahedron Lett.* **1999**, *40*, 1641−1644. Ozaki, S.; Yang, H. J.; Matsui, T.; Goto, Y.; Watanabe, Y. *Tetrahedron: Asymmetry* **1999**, *10*, 183−192. Manoj, K. M.; Hager, L. P. *Biochim. Biophys. Acta* **2001**, *1547*, 408−417.

(9) Suslick, K. S. In *The Porphyrin Handbook*; Kadish, K. M., Smith, K. M., Guilard, R., Eds.; Academic Press: San Diego, 2000; Vol. 4, pp 41−64.

(10) Vaz, A. D. N.; McGinnity, D. F.; Coon, M. J. *Proc. Natl. Acad. Sci. U.S.A.* **1998**, *95*, 3555−3560.

(11) Poulos, T. L. In *The Porphyrin Handbook*; Kadish, K. M., Smith, K. M., Guilard, R., Eds.; Academic Press: San Diego, 2000; Vol. 4, pp 189−218.

(12) Watanabe, Y. In *The Porphyrin Handbook*; Kadish, K. M., Smith, K. M., Guilard, R., Eds.; Academic Press: San Diego, 2000; Vol. 4, pp 97−118.

10.1021/ic0490122 CCC: $30.25
Published on Web 12/24/2004

In particular, proximal residues, such as histidine or cysteine, facilitate the O−X bond cleavage by providing electrons to the antibonding O−X orbital through the transition metal center (the push effect), whereas properly positioned distal residues shuttle the protons to the oxidant creating a good leaving group for the O−X bond heterolysis (the pull effect).[11,12] Although the enzymes ensure heterolysis of the O−X bond of the oxidants, the subsequent enantioselective oxygenation is presently impractical due to the restricted scope of the substrates and limited stability of the enzymes.[2,3,14−18] Therefore, synthetic catalysts, mimicking the enzymes, present more practical and often competitive alternative.

The transition metal complexes with chiral porphyrin and Schiff base ligands are among the best synthetic catalysts for the enantioselective oxygenation.[14,15] However, numerous studies have demonstrated that catalyst-assisted O−X bond cleavage does not ensure heterolysis.[12,14−17,19−22] Furthermore, oxygenation might proceed concertedly with the O−X bond cleavage, as opposed to stepwise O−O bond cleavage followed by oxygen transfer.[10,15,17,21,23,24] The actual mechanism and the mode of the O−X cleavage depend on the axial ligand, acidity of the media, and solvent employed during the reaction. Different experimental conditions, therefore, lead to different oxygenating species and hence diverse selectivity. To gain control over the oxygenating species, and subsequently the selectivity of catalytic oxygenation, careful investigation of the axial ligand (the push effect), protonation (the pull effect), and solvent effects is essential.

For this study we choose, without loss of generality, one of the best catalytic systems for enantioselective epoxidation utilizing Mn^{III} complex with chiral Schiff base salen ligand, namely the Kochi−Jacobsen−Katsuki (KJK) system.[2−5] The KJK system is generally believed to employ the transient high-valent Mn^{V}(O) species for productive enantioselective oxygenation.[25−31] Nevertheless, adducts of the terminal oxidants (such as peracids, iodozylarenes, etc.) and the KJK catalyst have been proposed as alternative oxygenating species in cases where dramatic deviations of the enantioselectivity occur.[4,18,24,32] Therefore, the mechanism of the O−X bond cleavage forming Mn^{V}(O) deserves special attention. Very recently formation of the Mn^{V}(O) species was studied theoretically for OCl− and H_2O_2 terminal oxidants.[33] Earlier, we investigated formation of the Mn^{V}(O) species in the KJK system by employing peracids as terminal oxidants and lately elaborated the push effect of the N and O bound axial ligands along with the solvent effect on the O−O bond activation.[28,29,31]

This paper reports the missing link in the control of the O−O bond activation—the pull effect, mimicked by protonation, concurrent with the push and solvent effects in the KJK system using peracid as terminal oxidant. The axial ligands imidazole and acetate are modeled by neutral NH_3 and anionic HCO_2^-, respectively. Where appropriate we use

(13) Harris, D. L. *Curr. Opin. Chem. Biol.* **2001**, *5*, 724−735.
(14) Groves, J. T.; Watanabe, Y.; McMurry, T. J. *J. Am. Chem. Soc.* **1983**, *105*, 4489−4490.
(15) Groves, J. T.; Watanabe, Y. *J. Am. Chem. Soc.* **1986**, *108*, 7834−7836.
(16) Collman, J. P.; Brauman, J. I.; Meunier, B.; Hayashi, T.; Kodadek, T.; Raybuck, S. A. *J. Am. Chem. Soc.* **1985**, *107*, 2000−2005. Groves, J. T.; Watanabe, Y. *J. Am. Chem. Soc.* **1988**, *110*, 8443−8452. Nam, W.; Han, H. J.; Oh, S.-Y.; Lee, Y. J.; Choi, M.-H.; Han, S.-Y.; Kim, C.; Woo, S. K.; Shin, W. *J. Am. Chem. Soc.* **2000**, *122*, 8677−8684.
(17) Watanabe, Y.; Yamaguchi, K.; Morishima, I.; Takehira, K.; Shimizu, M.; Hayakawa, T.; Orita, H. *Inorg. Chem.* **1991**, *30*, 2581−2582. Yamaguchi, K.; Watanabe, Y.; Morishima, I. *Inorg. Chem.* **1992**, *31*, 156−157. Yamaguchi, K.; Watanabe, Y.; Morishima, I. *J. Chem. Soc., Chem. Commun.* **1992**, 1709−1710. Yamaguchi, K.; Watanabe, Y.; Morishima, I. *J. Am. Chem. Soc.* **1993**, *115*, 4058−4065.
(18) Imagawa, K.; Nagata, T.; Yamada, T.; Mukaiyama, T. *Chem. Lett.* **1994**, 527−530. Mukaiyama, T.; Yamada, T. *Bull. Chem. Soc. Jpn.* **1995**, *68*, 17−35.
(19) Groves, J. T.; Watanabe, Y. *J. Am. Chem. Soc.* **1986**, *108*, 7836−7837. Groves, J. T.; Watanabe, Y. *Inorg. Chem.* **1987**, *26*, 785−786. Weiss, R.; Gold, A.; Trautwein, A. X.; Terner, J. In *The Porphyrin Handbook*; Kadish, K. M., Smith, K. M., Guilard, R., Eds.; Academic Press: San Diego, 2000; Vol. 4, pp 65−96. Bruice, T. C.; Balasubramanian, P. N.; Lee, R. W.; Smith, J. R. L. *J. Am. Chem. Soc.* **1988**, *110*, 7890−7892. Lee, W. A.; Bruice, T. C. *J. Am. Chem. Soc.* **1985**, *107*, 513−514. Panicucci, R.; Bruice, T. C. *J. Am. Chem. Soc.* **1990**, *112*, 6063−6071. Yuan, L.-C.; Bruice, T. C. *Inorg. Chem.* **1985**, *24*, 986−987. Yuan, L.-C.; Bruice, T. C. *J. Am. Chem. Soc.* **1986**, *108*, 1643−1650. Traylor, T. G.; Lee, W. A.; Styned, D. V. *J. Am. Chem. Soc.* **1984**, *106*, 755−764. Traylor, T. G.; Popovitz-Biro, R. *J. Am. Chem. Soc.* **1988**, *110*, 239−243. Traylor, T. G.; Xu, F. *J. Am. Chem. Soc.* **1990**, *112*, 178−186. Robert, A.; Loock, B.; Momenteau, M.; Meunier, B. *Inorg. Chem.* **1991**, *30*, 706−711. Nam, W.; Kim, I.; Lim, M. H.; Choi, H. J.; Lee, J. S.; Jang, H. G. *Chem.—Eur. J.* **2002**, *8*, 2067−2071. Chang, C. J.; Chng, L. L.; Nocera, D. G. *J. Am. Chem. Soc.* **2003**, *125*, 1866−1876.
(20) Groves, J. T.; Watanabe, Y. *Inorg. Chem.* **1986**, *25*, 4808−4810.
(21) Nam, W.; Lim, M. H.; Lee, H. J.; Kim, C. *J. Am. Chem. Soc.* **2000**, *122*, 6641−6647. Collman, J. P.; Chien, A. S.; Eberspacher, T. A.; Brauman, J. I. *J. Am. Chem. Soc.* **2000**, *122*, 11098−11100.
(22) Zipplies, M. F.; Lee, W. A.; Bruice, T. C. *J. Am. Chem. Soc.* **1986**, *108*, 4433−4445.
(23) Adam, W.; Mock-Knoblauch, C.; Saha-Moeller, C. R.; Herderich, M. *J. Am. Chem. Soc.* **2000**, *122*, 9685−9691. Adam, W.; Roschmann, K. J.; Saha-Moeller, C. R.; Seebach, D. *J. Am. Chem. Soc.* **2002**, *124*, 5068−5073. Bryliakov, K. P.; Khavrutskii, I. V.; Talsi, E. P.; Kholdeeva, O. A. *React. Kinet. Catal. Lett.* **2000**, *71*, 183−191. Linde, C.; Koliai, N.; Norrby, P.-O.; Akermark, B. *Chem.—Eur. J.* **2002**, *8*, 2568−2573.
(24) Collman, J. P.; Zeng, L.; Brauman, J. I. *Inorg. Chem.* **2004**, *43*, 2672−2679.
(25) Srinivasan, K.; Michaud, P.; Kochi, J. K. *J. Am. Chem. Soc.* **1986**, *108*, 2309−2320.
(26) Jepsen, A. S.; Roberson, M.; Hazell, R. G.; Jorgensen, K. A. *Chem. Commun.* **1998**, 1599−1600. Linde, C.; Aakermark, B.; Norrby, P.-O.; Svensson, M. *J. Am. Chem. Soc.* **1999**, *121*, 5083−5084. Cavallo, L.; Jacobsen, H. *Angew. Chem., Int. Ed.* **2000**, *39*, 589−592. Cavallo, L.; Jacobsen, H. *Eur. J. Inorg. Chem.* **2003**, 892−902. Cavallo, L.; Jacobsen, H. *J. Phys. Chem. A* **2003**, *107*, 5466−5471. Cavallo, L.; Jacobsen, H. *J. Org. Chem.* **2003**, *68*, 6202−6207. Jacobsen, H.; Cavallo, L. *Chem.—Eur. J.* **2001**, *20*, 1533−1544. El-Bahraoui, J.; Wiest, O.; Feichtinger, D.; Plattner, D. A. *Angew. Chem., Int. Ed.* **2001**, *40*, 2073−2076. Plattner, D. A.; Feichtinger, D.; El-Bahraoui, J.; Wiest, O. *Int. J. Mass Spectrom.* **2000**, *195/196*, 351−362. Strassner, T.; Houk, K. N. *Org. Lett.* **1999**, *1*, 419−421. Houk, K. N.; DeMello, N. C.; Condorski, K.; Fennen, J.; Kasuga, T. *Proc. ECHET96 Electron. Conf.* **1996**.
(27) Abashkin, Y. G.; Collins, J. R.; Burt, S. K. *Inorg. Chem.* **2001**, *40*, 4040−4048.
(28) Khavrutskii, I. V.; Rahim, R. R.; Musaev, D. G.; Morokuma, K. *J. Phys. Chem. B* **2004**, *108*, 3845−3854.
(29) Khavrutskii, I. V.; Musaev, D. G.; Morokuma, K. *J. Am. Chem. Soc.* **2003**, *125*, 13879−13889.
(30) Khavrutskii, I. V.; Musaev, D. G.; Morokuma, K. *Inorg. Chem.* **2003**, *42*, 2606−2621.
(31) Khavrutskii, I. V.; Musaev, D. G.; Morokuma, K. *Proc. Natl. Acad. Sci. U.S.A.* **2004**, *101*, 5743−5748.
(32) Palucki, M.; Finney, N. S.; Pospisil, P. J.; Gueler, M. L.; Ishida, T.; Jacobsen, E. N. *J. Am. Chem. Soc.* **1998**, *120*, 948−954.
(33) Cavallo, L.; Jacobsen, H. *Inorg. Chem.* **2004**, *43*, 2175−2182. Abashkin, Y. G.; Burt, S. K. *J. Phys. Chem. B.* **2004**, *108*, 2708−2711.

acetonitrile and toluene as solvent to account for polar and nonpolar solvent effects.

II. Computational Methods

All calculations were performed with the Gaussian03 (G03) program suite.[34] This study utilized density functional theory (DFT), in particular Becke's three-parameter hybrid exchange functional (B3)[35,36] combined with Lee−Yang−Parr's (LYP) correlation functional,[37] known as B3LYP. We refrain from using the nonhybrid BP86 and BPW91 methods which combine the Becke88 exchange (B)[35] and Perdew86 (P86) or the Perdew−Wang gradient-corrected correlation (PW91) functionals[38] despite recent comparison of the representative hybrid and nonhybrid DFT methods against CCSD-(T) advocating nonhybrid variants for Mn transition metal systems.[27] Our choice is based on the invalidation of that comparison as discussed elsewhere[30] and further supported by independent comparison of the referred methods on the series of Fe and Mn transition metal complexes with known ground states.[28−30,39] Moreover, apparent failure of the BP86 and BPW91 methods to describe the O−O bond breaking demonstrated previously[28] renders these methods particularly unusable when reaction mechanisms are to be studied. The double-ζ LANL2DZ (D95V[40]) basis set with associated Hay−Wadt nonrelativistic effective core potential (ECP) on the Mn was employed for the present calculations.[41] All geometries were optimized without any constraints, using tight optimization and SCF convergence threshold of 10^{-8}. Due to large system size, vibrational frequency calculations were performed only for the transition states to confirm their nature and presence of single imaginary frequency. Therefore, the energy values used hereafter are without zero-point energy and entropy corrections. The solvent effect was incorporated using polarized continuum model (PCM) method as implemented in G03[42] at gas-phase optimized structures.

Chart 1. Explanation of Notation for Acylperoxo Complexes and Labeling of the Atoms with Proton Locations Not Specified for Clarity

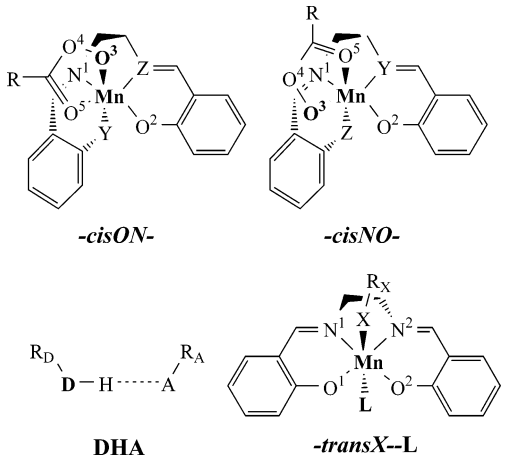

III. Results and Discussion

This section is organized as follows. Part A discusses the protonation and axial ligand effects on the electronic and geometric structure of the acylperoxo complexes [(Salen)-$Mn^{III}(RCO_3H)L$] and [(SalenH)$Mn^{III}(RCO_3)L$] with L = none, NH_3, and HCO_2^-. Part B elucidates the pull and push effects on the O−O bond activation in the protonated acylperoxo complexes. Part C elaborates the nature of the obtained intermediates and illuminates aprotic solvents effect. The final part D compares the O−O bond cleavage pathways in the protonated and unprotonated complexes.

Throughout the paper we exploit the mnemonic notation of compounds and atom numbering, depicted in Chart 1, adopted from previous work[28,29,31] but augmented for hydrogen bond pattern: Mn^N-A^{2S+1}-*cisYZ*-DHA and Mn^N-A^{2S+1}-*transX*-DHA-L, where *N* reflects the oxidation state of the Mn atom, $^{2S+1}$A describes the symmetry and spin multiplicity of the system, *Y* and *Z* stand for the atoms of the Salen ligand situated trans to peroxo oxygen O^3 and carbonyl oxygen O^5 of the acylperoxo ligand, respectively, and *X* is the atom of the peracid coordinated to the Mn. Unless otherwise stated, the atoms Y and Z are O^1 or N^2 and the puckered ethylene diimine bridge is in λ configuration. The DHA label describes the location of hydrogen and possible hydrogen bonding, with D denoting the hydrogen donor and A the hydrogen acceptor, if any. For example, when an intra-peracid hydrogen bond is present, this notation becomes O^3HO^5. Finally, L represents an exogenous ligand. Note that for the trans isomer the *X* atom of the peracid becomes chiral (because now in addition to the lone pair it has three different substituents, namely Mn, H, and either carbonyl carbon or oxygen atoms) and, furthermore, several rotamers exist due to hindered rotation around the MnX axis. Because no new qualitative rearrangement of atoms is found and because the diastereomers/rotamers differ only slightly in energy (data not shown), we

(34) Frisch, M. J.; Trucks, G. W.; Schlegel, H. B.; Scuseria, G. E.; Robb, M. A.; Cheeseman, J. R.; J. A. Montgomery, J.; Vreven, T.; Kudin, K. N.; Burant, J. C.; Millam, J. M.; Iyengar, S. S.; Tomasi, J.; Barone, V.; Mennucci, B.; Cossi, M.; Scalmani, G.; Rega, N.; Petersson, G. A.; Nakatsuji, H.; Hada, M.; Ehara, M.; Toyota, K.; Fukuda, R.; Hasegawa, J.; Ishida, M.; Nakajima, T.; Honda, Y.; Kitao, O.; Nakai, H.; Klene, M.; Li, X.; Knox, J. E.; Hratchian, H. P.; Cross, J. B.; Adamo, C.; Jaramillo, J.; Gomperts, R.; Stratmann, R. E.; Yazyev, O.; Austin, A. J.; Cammi, R.; Pomelli, C.; Ochterski, J. W.; Ayala, P. Y.; Morokuma, K.; Voth, G. A.; Salvador, P.; Dannenberg, J. J.; Zakrzewski, V. G.; Dapprich, S.; Daniels, A. D.; Strain, M. C.; Farkas, O.; Malick, D. K.; Rabuck, A. D.; Raghavachari, K.; Foresman, J. B.; Ortiz, J. V.; Cui, Q.; Baboul, A. G.; Clifford, S.; Cioslowski, J.; Stefanov, B. B.; Liu, G.; Liashenko, A.; Piskorz, P.; Komaromi, I.; Martin, R. L.; Fox, D. J.; Keith, T.; Al-Laham, M. A.; Peng, C. Y.; Nanayakkara, A.; Challacombe, M.; Gill, P. M. W.; Johnson, B.; Chen, W.; Wong, M. W.; Gonzalez, C.; Pople, J. A. *Gaussian03*, revision B.1 ed.; Gaussian, Inc.: Pittsburgh, PA, 2003.
(35) Becke, A. D. *Phys. Rev. A: At., Mol., Opt. Phys.* **1988**, *38*, 3098−3100.
(36) Becke, A. D. *J. Chem. Phys.* **1993**, *98*, 5648−5652.
(37) Lee, C.; Yang, W.; Parr, R. G. *Phys. Rev. B: Condens. Matter Mater. Phys.* **1988**, *37*, 785.
(38) Perdew, J. P. *Phys. Rev. B: Condens. Matter Mater. Phys.* **1986**, *33*, 8822−8824. Perdew, J. P.; Chevary, J. A.; Vosko, S. H.; Jackson, K. A.; Pederson, M. R.; Fiolhais, C. *Phys. Rev. B: Condens. Matter Mater. Phys.* **1992**, *46*, 6671−6687.
(39) Quiñonero, D.; Musaev, D. G.; Morokuma, K. *Inorg. Chem.* **2003**, *42*, 8449−8455. Khoroshun, D. V.; Musaev, D. G.; Vreven, T.; Morokuma, K. *Organometallics* **2001**, *20*, 2007−2026. Lundberg, M.; Blomberg, M. R. A.; Siegbahn, P. E. M. *Inorg. Chem.* **2004**, *43*, 264−274.
(40) Dunning, T. H.; Hay, P. J. In *Modern Theoretical Chemistry*; Schaefer, H. F., III, Ed.; Plenum: New York, 1977; Vol. 3, pp 1−27.
(41) Hay, P. J.; Wadt, W. R. *J. Chem. Phys.* **1985**, *82*, 270−283. Hay, P. J.; Wadt, W. R. *J. Chem. Phys.* **1985**, *85*, 299−310.
(42) Mennucci, B.; Tomasi, J. *J. Chem. Phys.* **1997**, *106*, 5151−5158. Cances, E.; Mennucci, B.; Tomasi, J. *J. Chem. Phys.* **1997**, *107*, 3032−3041. Cossi, M.; Barone, V.; Mennucci, B.; Tomasi, J. *Chem. Phys. Lett.* **1998**, *286*, 253−260. Cossi, M.; Scalmani, G.; Rega, N.; Barone, V. *J. Chem. Phys.* **2002**, *117*, 43−54.

focus our attention on the transformations of the lowest energy isomers and assume the transformations of the diastereomers/rotamers to be similar. We have verified our assumption in a few cases for the least intuitive cases of diastereomers and found the assumption to be correct (data not shown for brevity). Because this paper considers only acylperoxo complexes of Mn^{III}, the Mn^{N} part of the label is omitted.

A. Complexes [(Salen)Mn^{III}(RCO$_3$H)L] and [(SalenH)-Mn^{III}(RCO$_3$)L]. This section describes the geometric and electronic properties of the protonated acylperoxo complexes [(Salen)Mn^{III}(RCO$_3$H)L] and [(SalenH)Mn^{III}(RCO$_3$)L] with L = none, NH_3, and HCO_2^-.[43] Because the unprotonated acylperoxo complexes in the quintet and triplet spin states have been established to have similar geometries,[28,29,31] the search for the structure of the protonated acylperoxo complexes is first performed in the high-spin quintet state. Once the principal geometric isomers of the protonated complexes have been identified, their energies in the quintet and triplet states are compared. To focus on the energetics of a large number of isomers, we completely omit discussions on their geometrical structures, except for Figure 1 that illustrates the structures of some of the *transO*-NH_3 species. Key geometrical parameters and spin densities of all the calculated species are summarized in Tables 1S and 2S of the Supporting Information, along with Cartesian coordinates.

L = None. The obvious way to generate the structure of the protonated acylperoxo complex is to coordinate a peracid to the Mn center of the catalyst preserving intra-peracid hydrogen bond O^3HO^5. This approach produces *transO*^{3}-O^3-HO^5-L and *transO*^{5}-O^3HO^5-L complexes degenerate in energy in the quintet state. For convenience the *transO*^{3}-O^3-HO^5-L complex in the quintet state is used as the reference compound in the following paragraphs.

Adding a proton to the unprotonated acylperoxo complexes may lead to additional geometric isomers of the protonated acylperoxo complexes. The most likely proton acceptors in the *cisON*, *cisNO*, and *transO*^{3} isomers of the unprotonated acylperoxo complexes are the sp^3 oxygen atoms of the Salen ligand (O^1 and O^2) and coordinated acylperoxo anion (O^3) as seen from Chart 1. The protonation of the referred oxygen atoms should produce [(SalenH)Mn^{III}(RCO$_3$)L] and [(Salen)-Mn^{III}(RCO$_3$H)L] complexes, respectively.

The protonation of the Salen oxygens of the cis acylperoxo complexes yields four protonated complexes, namely *cisNO*-O^1H, *cisNO*-O^2H, *cisON*-O^1H, and *cisON*-O^2H. As shown in Table 1, the relative energies of these complexes in the quintet state are −2.4, 6.1, 1.4, and 3.2 kcal/mol, respectively. On the other hand, protonation of the Salen oxygens of the *transO*^{3} complex triggers isomerization into familiar *cisNO*-O^1H (−2.4 kcal/mol) and a new *cisN*^{1}*O*^{2}-O^2H (1.5 kcal/mol) complex. Because the latter isomer is enantiomeric to *cisNO*-O^1H but has the diimine bridge in δ-configuration, the change in configuration of the diimine bridge from λ to δ for *cisNO*-O^1H is inferred to be 3.9 kcal/mol unfavorable. The *cisNO*-O^1H complex has the lowest energy among all cis isomers in the gas phase. The solvent effect on the relative energies of the complexes is small, as seen in the values in parentheses in Table 1. (The first entry corresponds to toluene, and the second, to acetonitrile solvent.)

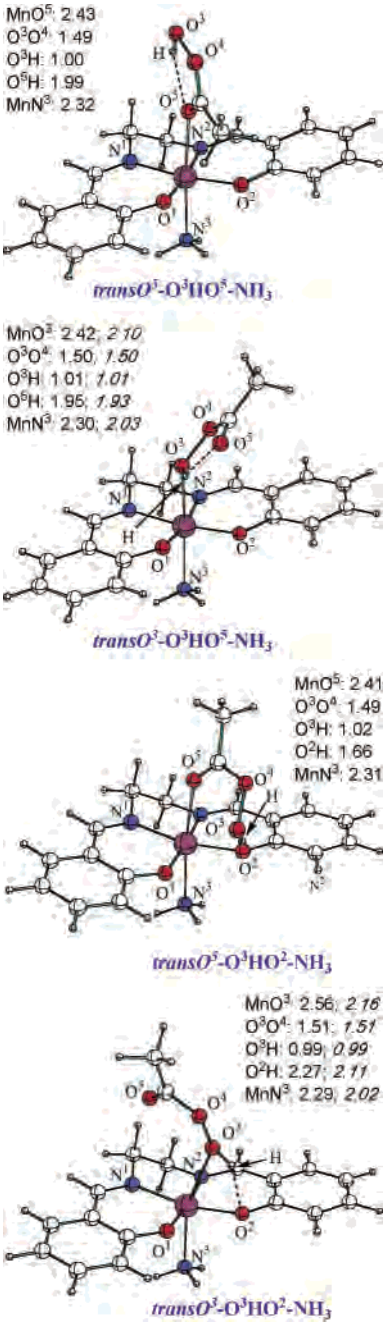

Figure 1. Four representative protonated trans acylperoxo complexes for L = NH_3 and their key bond lengths. Plain numbers refer to the quintet ground state, and numbers in italics refer to the triplet state.

Interestingly, protonation of the *cisON* and *cisNO* complexes at the peroxo oxygen O^3 produces new *transO*^{5}-O^3H and *transO*^{5}-O^3HO^2 complexes with the −4.2 and −6.0 kcal/mol relative energies, respectively. On the other hand, protonation of the O^3 in trans acylperoxo complex generates the *transO*^{3}-O^3HO^2 isomer with −1.7 kcal/mol relative energy. Comparing the energy differences between *transO*^{5}-

(43) The O−O bond cleavage in the protonated cis acylperoxo complexes is expected to be similar to that in corresponding unprotonated cis complexes,[29] although with the reduced efficiency due to increased triplet−quintet energy gap (as discussed above).

Table 1. Relative and Binding Energies (in kcal/mol) for Protonated Acylperoxo Complexes[a]

complex	state	relative energy		
		L = none	L = NH_3	L = HCO_2^-
transO^3-O^{3}HO^5-L	^{5}A	0.0 (0.0, 0.0)	0.0 (0.0, 0.0)	0.0 (0.0, 0.0)
	^{3}A	29.8	10.4	11.5
transO^3-O^{3}HO^2-L	^{5}A	−1.7 (−2.1, −2.3)	−1.8	does not exist
	^{3}A		11.8	11.7
transO^5-O^{3}HO^2-L	^{5}A	−6.0 (−5.8, −4.4)	−4.5 (−4.9, −5.1)	−6.2 (−5.6, −5.8)
transO^5-O^{3}HO^5-L	^{5}A	0.0 (−0.8, −0.9)	1.2	0.1
transO^5-O^{3}H-L	^{5}A	−4.2	−2.5	0.9
transO^3-O^{1}H-L[b]	^{5}A	−2.4 (−3.7, −4.4)	13.9	
cisNO-O^{1}H-L	^{3}A	12.7		
transO^3-O^{2}H-L[c]	^{5}A	1.5 (1.1, 0.3)	14.7	
cisNO-O^{2}H-L	^{5}A	6.1 (6.4, 7.0)		
cisON-O^{1}H-L	^{5}A	1.4 (−0.5, −1.6)		
cisON-O^{2}H-L	^{5}A	3.2 (2.6, 3.3)		

complex	state	binding energy: {*i*:*j*}[d]				
		[ML]−RCO_3H {1:0}	[ML]−RCO_3H {1:0}	[MR]−L {1:0}	[ML]−RCO_3H {0:0}	[MR]−L {1:−1}
transO^3-O^{3}HO^5-L	^{5}A	16.9 (9.3, −0.1)	11.6 (6.4, 0.3)	21.3 (19.6, 16.2)	8.2 (5.1, 1.5)	114.7 (58.2, 19.2)
transO^3-O^{3}HO^2-L	^{5}A	18.6 (11.4, 2.2)				
transO^5-O^{3}HO^5-L	^{5}A	16.9 (10.0, 0.8)				
transO^5-O^{3}HO^2-L	^{5}A	22.9 (15.1, 4.3)	16.0 (11.3, 5.4)	19.7 (18.8, 16.9)	14.0 (10.7, 7.3)	114.4 (58.0, 20.6)

[a] The first and second numbers in parentheses are the relative or binding energies in toluene and acetonitrile solvents, respectively. For L = none. [b] *transO*^{3}-O^{1}H converged to *cisNO*-O^{1}H. [c] *transO*^{3}-O^{2}H converged to *cisN*^{1}*O*^{2}-O^{2}H. [d] In {*i*:*j*} the *i* and *j* show the total charge of the first and second dissociation fragments, respectively.

O^{3}HO^2 and *transO*^{5}-O^{3}HO^5 and also between *transO*^{3}-O^3-HO^2 and *transO*^{3}-O^{3}HO^5 shows that destroying the intraperacid O^3-H···O^5 hydrogen bond and creating the peracid−Salen O^3-H···O^2 hydrogen bond is 6.0 and 1.7 kcal/mol favorable, for *transO*^{5} and *transO*^{3} species, respectively.

The lowest energy triplet state of trans complexes is 29.8 kcal/mol higher than the quintet state. Even in the cis complexes, where the triplet state is expected to be closer to the ground state,[28,29,31] the triplet−quintet energy gap is significant. Specifically, for the *cisNO*-O^{1}H isomer the triplet−quintet gap is 15.1 kcal/mol, a substantial increase from the 9.7 kcal/mol gap in the unprotonated *cisNO* isomer.[29] Therefore, the ground state of the protonated acylperoxo complexes with L = none is the quintet state.

L = NH_3 and HCO_2^-. Because axial ligand L precludes isomerization of the trans acylperoxo complexes into cis isomers, only six protonated acylperoxo complexes, namely *transO*^{3}-O^{3}HO^5-L, *transO*^{3}-O^{3}HO^2-L, *transO*^{5}-O^{3}HO^5-L, *transO*^{5}-O^{3}HO^2-L, *transO*^{3}-O^{1}H-L, and *transO*^{3}-O^{2}H-L have been identified. Similar to the L = none case, the quintet state *transO*^{5}-O^{3}HO^2-L isomer is found to have the lowest energy in the presence of the axial ligands. Relative to the complex *transO*^{3}-O^{3}HO^5-L, the energies of the *transO*^{5}-O^{3}HO^2-L complex are −4.5 and −6.2 kcal/mol for L = NH_3 and L = HCO_2^-, respectively, as shown in Table 1. For L = NH_3 the relative energy of the reactive *transO*^{3}-O^{3}HO^2-L complex is −1.8 kcal/mol, while for L = HCO_2^- this complex does not exist. The energies of the isomers *transO*^{3}-O^{1}H and -O^{2}H are 13.9 and 14.7 kcal/mol, respectively for L = NH_3, indicating that protonation of the Salen oxygen atoms O^1 and O^2 in the specified configuration is strongly unfavorable.

Axial ligand coordination substantially reduces the triplet−quintet energy gap in the protonated acylperoxo complexes. Nevertheless, the triplet state complexes are still higher in energy than the corresponding quintet state complexes. Therefore, the ground state of the protonated *transX*-L complexes remains to be the quintet state. For example the triplet−quintet energy gap in *transO*^{3}-O^{3}HO^5-L isomer reduces from 29.8 kcal/mol for L = none to 10.4 and 11.5 kcal/mol for L = NH_3 and HCO_2^-, respectively. Note that the difference in stabilization of the triplet state by NH_3 and HCO_2^- predicted by B3LYP is in agreement with the spectrochemical order of the two ligands.[44] The relatively small triplet−quintet energy gap in protonated acylperoxo complexes with L = NH_3 and HCO_2^- suggests that the triplet state should also be considered when studying the O−O bond activation in these complexes.

Stability of the Protonated Complexes. The stability of the protonated acylperoxo complexes with respect to dissociation in solution has been assessed on the basis of computed binding energies between Mn^{III}SalenL catalyst and peracetic acid ([ML]−RCO_3H), and also between the Mn^{III}-SalenRCO_3H and L ([MR]−L), which are summarized in the bottom of Table 1. There for clarity we indicated the actual charges of the two dissociation fragments in the brace {*i*:*j*}, with *i* being the charge of the bracket fragment. As seen from the Table 1, the binding energies of neutral RCO_3H to Mn^{III}SalenL catalyst rapidly decrease with increasing solvent polarity, suggesting that the [ML]−RCO_3H complex is likely to dissociate in polar solvents. Although binding energies of L follow the same trend, they remain relatively large even in the acetonitrile.

B. O−O Bond Cleavage in [(Salen)Mn^{III}(RCO_3H)L] Acylperoxo Complexes. The following part describes the O−O bond cleavage in the *transO*^{3}-O^{3}HO^5-L and *transO*^{3}-O^{3}HO^2-L with L = none, NH_3, and HCO_2^-, in which peracid is coordinated to the metal via protonated peroxo oxygen

(44) Shimura, Y.; Tsuchida, R. *Bull. Chem. Soc. Jpn.* **1955**, *29*, 311−316. Piquemal, J.-P.; Williams-Hubbard, B.; Fey, N.; Deeth, R. J.; Gresh, N.; Giessner-Prettre, C. *J. Comput. Chem.* **2003**, *24*, 1963−1970.

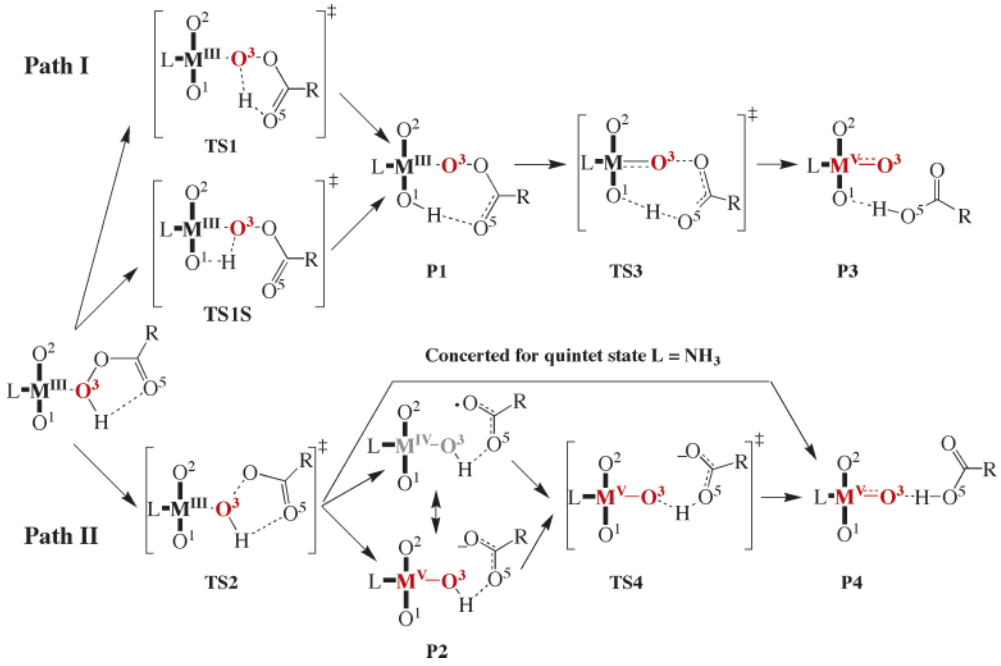

Figure 2. Schematic representation of the pathways I and II for the O−O bond cleavage in Mn^{III}−*transO*^{3}-O^{3}HO^5-L. The scheme does not reflect changes in the spin states along the reaction pathways (see text for details).

O^3. The O−O bond cleavage in the cis acylperoxo complexes protonated at Salen oxygen atoms O^1 or O^2 should be similar to that in corresponding unprotonated complexes.[29] However, the protonation of the Salen oxygens increases the triplet−quintet energy gap in the cis complexes, rendering them less efficient in the O−O bond cleavage.[29] For this reason we do not consider the O−O bond cleavage in the protonated cis complexes.

The O−O bond cleavage in the protonated *transO*^{3}-L complexes follows two new pathways. Figure 2 illustrates the simplified mechanism for the representative *transO*^{3}-O^{3}HO^5-L case.

The pathway I starts with hydrogen transfer from O^3 to either carbonyl O^5 or Salen O^1 oxygen atoms via the transition state TS1 or TS1S, respectively. Interestingly, both hydrogen transfers produce the same intermediate P1, from which concerted heterolytic O−O bond cleavage coupled to hydrogen transfer from O^1 to O^5 via the transition state TS3 completes the pathway I. The pathway II, on the other hand, starts with pure O−O bond cleavage via the transition state TS2, followed by hydrogen abstraction from O^3 by O^5 oxygen to generate carboxylic acid. Depending on the axial ligand and the spin state of the complex, the latter step has no or very small barrier at TS4. Note that the O−O bond cleavage in acylperoxo complexes can also produce *N*-oxides.[28,29] Generally, such cleavage only occurs in the high-spin (quintet) complexes and is more likely in *cis*- than *transO*^{3}-L acylperoxo complexes.[28,29] However, this pathway still requires high activation energy and is not considered here.

Because several geometric isomers of the protonated acylperoxo complexes presumably coexist in equilibrium, it is important to know the relative energies of the isomers capable of the O−O bond cleavage, with respect to the most thermodynamically stable unreactive isomer. In part A, we already identified the *transO*^{5}-O^{3}HO^2-L isomers as the most thermodynamically stable. Relative to these isomers the energies of the reactive *transO*^{3}-O^{3}HO^5-L complexes in the quintet state are 6.0, 4.5, and 6.2 kcal/mol for L = none, NH_3, and HCO_2^-, respectively. The relative energy of the other reactive isomer *transO*^{3}-O^{3}HO^2-L is 4.3 and 2.7 kcal/mol, for L = none and NH_3.

O−O Bond Cleavage in the *transO*^{3}-O^{3}HO^5-L Acylperoxo Complex. Quintet Pathway I. As seen from Table 2 and Figure 3, the energies of the quintet state hydrogen transfer transition state TS1 are 9.3, 11.6, and 15.8 kcal/mol, whereas those of the TS1S are 16.0, 14.4, and 11.5 kcal/mol, for L = none, NH_3, and HCO_2^-, respectively. Clearly in the absence of the axial ligand, it is easier to shuttle a proton to the carbonyl oxygen O^5 than to the Salen oxygen O^1, but this can be reversed by the axial ligand. Interestingly, once the proton is transferred to the carbonyl O^5 oxygen via TS1, we find that the peracid spontaneously (exothermically without barrier) rotates and then shuttles its hydrogen from O^5 to the O^1, giving the intermediate P1, which is identical with the intermediate obtained by the direct proton transfer to the Salen oxygen O^1 via TS1S. The relative energies of the intermediate P1 are −1.2, 0.7, and −1.7 kcal/mol with respect to the starting acylperoxo complexes *transO*^{3}-O^{3}HO^5-L, for L = none, NH_3, and HCO_2^-. Formally, the intermediate P1 can be considered as *transO*^{3}-O^{1}HO^5-L isomer of the protonated acylperoxo complex. Note that direct protonation of the O^1 in the *transO*^{3}-L complex produces *transO*^{3}-O^{1}H isomer, which is 13.2 kcal/mol higher in energy than P1 for L = NH_3 case. From the intermediate P1 the O−O bond can heterolytically cleave via the concerted TS3 with barriers of 15.6, 13.4, and 15.9 kcal/mol calculated from P1 for L = none, NH_3, and HCO_2^-, respectively. The final product P3 is [(Salen)Mn^V(O)L] hydrogen-bonded to RCO_2H. In this complex, for L = none, RCO_2H is hydrogen-bonded to the

Table 2. Relative Energies *E* (in kcal/mol) of Transition States and Intermediates for O−O Bond Cleavage Pathways I and II in Protonated Acylperoxo Complexes, *trans*O^3-O^3HO^5-L and *trans*O^3-O^3HO^2-L

species	state	L = none	L = NH_3	L = HCO_2^-
transO^3-O^3HO^5-L	^{5}A	0.0	0.0	0.0
TS1	^{5}A	9.3	11.6	15.8
	^{3}A		19.6	24.1
TS1S	^{5}A	16.0	14.4	11.5
	^{3}A		21.4	18.5
P1	^{5}A	−1.2	0.7	−1.7
	^{3}A		2.0	1.0
TS3	^{5}A	14.4	14.1	14.2
	^{3}A		6.6	6.3
P3	^{5}A	−1.4	−1.7	−9.1
	^{3}A		−0.1	−5.3
TS2	^{5}A	13.6	11.1	9.1
	^{3}A		16.0	16.1
P2	^{5}A	4.6		−2.2
	^{3}A		3.8	−3.3
TS4	^{5}A	4.6	no barrier	−1.1
	^{3}A		4.8	−2.0
P4	^{5}A	−1.4	−7.4	−13.4
	^{3}A		−4.9	−11.7
transO^3-O^3HO^2-L	^{5}A	−1.7	−1.8	does not exist
TS1S	^{5}A	11.7		
	^{3}A		21.0	
P1	^{3}A		15.9	
TS2	^{5}A	12.4	8.8	
	^{3}A		17.0	
P2	^{5}A	11.3	4.2	
	^{3}A		4.5	
TS2I	^{5}A	11.2		
P2I	^{5}A	−4.5		
A1[a]		198.0	182.8	111.2
		(98.5, 29.5)	(81.7, 9.5)	(44.9, 3.6)
A2[a]		17.6	11.0	6.9
		(13.3, 10.3)	(5.5, −0.1)	(4.0, 1.5)

[a] The first and second numbers in parentheses are the relative energies in toluene and acetonitrile solvents, respectively.

MnO^3 group, whereas, for L = NH_3 and HCO_2^-, RCO_2H hydrogen-bonds to the Salen O^1 and aligns in the plane with the Salen phenyl rings (not shown). The relative energy of the hydrogen-bonded P3 is −1.4, −1.7, and −9.1 kcal/mol for L = none, NH_3, and HCO_2^-, respectively.

Triplet Pathway I. On the basis of the triplet−quintet energy gap, the O−O bond cleavage in the triplet state is considered only for complexes with L = NH_3 and HCO_2^-. In the triplet state the activation energies for the first steps TS1 and TS1S are substantially higher than in the quintet state. For instance, the relative energies of the triplet TS1 are 19.6 and 24.1 kcal/mol and of TS1S are 21.4 and 18.5 kcal/mol for L = NH_3 and HCO_2^-, respectively. Nevertheless, the energy of the triplet intermediate P1 is close to the quintet state P1, namely 2.0 and 1.0 kcal/mol for L = NH_3 and HCO_2^-. Moreover, the relative energies of the subsequent O−O bond cleavage TS3 on the triplet state are substantially lower than on the quintet state, the situation similar to the O−O bond cleavage in the unprotonated *trans*O^3 complexes.[28,29] For example, the energy of TS3 is 6.6 and 6.3 kcal/mol, relative to the quintet *trans*O^3-O^3HO^5-L for L = NH_3 and HCO_2^-, respectively. Therefore, the spin crossover (intersystem crossing) from the quintet to triplet is likely to take place in the vicinity of the intermediate P1 (shown by wavy line in the Figure 3). The most likely route for pathway I is quintet reactant (*trans*O^3-O^3HO^5-L) → quintet TS1 → quintet P1 → triplet P1 → triplet TS3 → triplet P3 → quintet P3. The structure of the final triplet product P3 is similar to the quintet P3 and has [(Salen)Mn^V-(O)L] and RCO_2H associated by an O^5HO^1 hydrogen bond. The relative energy of the triplet P3 is −0.1 and −5.3 kcal/mol, for L = NH_3 and HCO_2^-. From spin density analysis (see Supporting Information) the [(Salen)Mn^V(O)L] fragment has been found to correspond to a broken-symmetry triplet state with three α unpaired electrons on Mn and one β electron on the O^3 atoms.

Quintet Pathway II. As seen from Table 2 and Figure 3, the barrier for initial O−O bond cleavage TS2 is 13.6, 11.1, and 9.1 kcal/mol, for L = none, NH_3, and HCO_2^-, respectively. In the L = NH_3 case, the O−O bond cleavage is followed by spontaneous hydrogen abstraction from O^3 by O^4 oxygen to form product P4 species, comprising [(Salen)-Mn^V(O)L] and RCO_2H. However, in the case of L = none and HCO_2^- the O−O bond cleavage results in an intermediate chameleon species P2, which can formally be described as either associated [(Salen)Mn^{IV}(OH)L] and RCO_2 radical or [(Salen)Mn^V(OH)L] and RCO_2^- anion. The relative energies of the chameleon intermediate are 4.6 and −2.2 kcal/mol for L = none and HCO_2^-, respectively. The chameleon nature of the product P2 will be discussed in more detail later. The barrier for the secondary hydrogen abstraction via TS4 from the chameleon intermediate P2 is negligible (<0.05 kcal/mol) for L = none and only 1.1 kcal/mol for L = HCO_2^-, respectively. This suggests that chameleon intermediate is likely to have very short lifetime. The final product of the pathway II-P4 differs from the final product of the pathway I-P3 only in the hydrogen bond pattern. In particular, in the product P4 with L = none, NH_3, and HCO_2^- the RCO_2H molecule is hydrogen bonded to the MnO^3 moiety. The relative energies of the P4 are lower than those of P3 and are −7.4, and −13.4 kcal/mol, for L = NH_3 and HCO_2^-, respectively. Therefore, the O^5HO^3 hydrogen bond in P4 is stronger than the O^5HO^1 bond in P3.

Triplet Pathway II. In the triplet state the activation energy for the O−O bond cleavage TS2 is higher than in the quintet state and is 16.0 and 16.1 kcal/mol for L = NH_3 and HCO_2^-, respectively. In contrast to the quintet state the triplet state intermediate P2 is formed in both L = NH_3 and HCO_2^- cases and has 3.8 and −3.3 kcal/mol relative energy, respectively. The relative energies of the hydrogen abstraction TS4 in the triplet state are 4.8 and −1.1 kcal/mol, for L = NH_3 and HCO_2^-, respectively. At least for L = HCO_2^- both the triplet intermediate P2 and the transition state TS4 are lower in energy than corresponding quintet species. Therefore, triplet pathway may interfere with the quintet pathway II.

O−O Bond Cleavage in the *trans*-O^3-O^3HO^2-L Acylperoxo Complex. The following paragraphs discuss the O−O bond cleavage in the *trans*O^3-O^3HO^2-L isomer of acylperoxo complexes (not shown in Figure 3), which is 1.7 and 1.8 kcal/mol lower than the *trans*O^3-O^3HO^5-L isomer discussed above, for L = none and NH_3, respectively. For L = HCO_2^- the peracid does not coordinate to the metal; instead it latches to the Salen oxygen with a hydrogen bond. In the *trans*O^3-O^3HO^2-L isomer the intra-peracid hydrogen

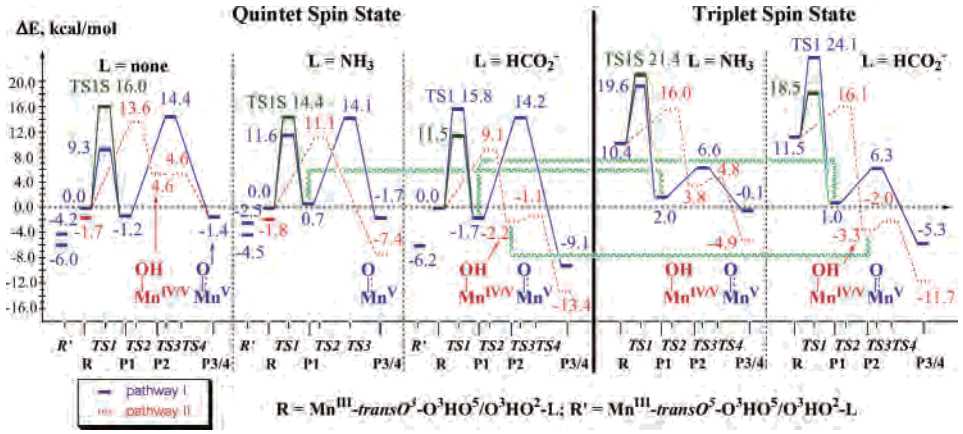

Figure 3. Energy diagram for the O−O bond cleavage in Mn^{III}−*transO*^{3}-O^{3}HO^5-L in the quintet and triplet states. The solid lines depict the pathway I profiles, whereas dashed lines depict the pathway II profiles. The wavy lines represent the most favorable spin-state transitions.

bond is missing, and therefore, direct hydrogen transfer from O^3 to O^5 is no longer possible.

Pathway I. The hydrogen transfer step occurs differently in the *transO*^{3}-O^{3}HO^2-L, in particular for the L = none case. In the case of L = none, the hydrogen atom transfers to the Salen O^2 oxygen via TS1S accompanied by isomerization to *cisN*^{1}*O*^{2}-O^{2}H complex with the diimine bridge in the *δ* configuration. The relative energy of the TS1S is 11.7 kcal/mol and the energy of the product acylperoxo complex *cisN*^{1}*O*^{2}-O^{2}H with *δ*-puckered diimine bridge is the same as that of its enantiomer *cisNO*-O^{1}H described in the preceding paragraphs (−2.4 kcal/mol). On the other hand for L = NH$_3$, the hydrogen transfer does not occur since the axial ligand precludes trans−cis isomerization and the transfer would result in the *transO*^{3}-O^{2}H-L acylperoxo complex, which has high relative energy of 14.7 kcal/mol (see above).

In the triplet state *transO*^{3}-O^{3}HO^2-L with L = NH$_3$, the relative energy of the hydrogen transfer TS1S is 21.0 kcal/mol. The product P1 also has high relative energy of 15.9 kcal/mol. Therefore, the triplet *transO*^{3}-O^{3}HO^2-L complex should not contribute to the reaction via pathway I.

Pathway II. The O−O bond cleavage in the isomer *transO*^{3}-O^{3}HO^2-L is also quite different from that in the *transO*^{3}-O^{3}HO^5-L complex. In particular, for L = none, we found two subpathways to cleave the O−O bond, namely with and without trans−cis isomerization. The relative energy of the transition state for the cleavage without isomerization, TS2, is 12.4 kcal/mol, whereas that with the isomerization, TS2I, is 11.2 kcal/mol. The TS2I results in the *cisN*^{1}*O*^{2} [(Salen)Mn^V(OH)RCO$_2^-$] hydroxy complex P2I, with *δ*-puckered diimine bridge, whereas the latter generates a new complex *transO*^{3}-O^{3}HO^2-L P2. The relative energies of the P2I and P2 are −4.5 and 11.3 kcal/mol, respectively. In the chameleon intermediate P2 from *transO*^{3}-O^{3}HO^2-L unlike in P2 from *transO*^{3}-O^{3}HO^5-L complex, the coupling of RCO$_2$ and [(Salen)Mn^{IV}(OH)] is through weak O^3···O^4 interaction rather than through the O^{3}HO^5 hydrogen bond. Therefore, immediate hydrogen abstraction step is precluded. However, hydrogen transfer from O^3 to O^4 or O^5 might still be possible after small rearrangements in the *transO*^{3}-O^{3}HO^5-L P2 intermediate. In contrast, in the *cisN*^{1}*O*^{2} hydrogen transfer from O^3 to O^4 is energetically unfavorable and the *cisN*^{1}*O*^{2} [(Salen)Mn^V(OH)RCO$_2^-$] hydroxy species P2I is the final product on the pathway II.

For the *transO*^{3}-O^{3}HO^2-L complex with L = NH$_3$ the relative energy of the quintet state O−O bond cleavage TS2 is 8.8 kcal/mol. The product P2 is similar to the P2 with L = none in the interaction between RCO$_2$ and [(Salen)Mn^{IV}-(OH)] and has relative energy of 4.2 kcal/mol. In the triplet *transO*^{3}-O^{3}HO^2-L complex the energy of the O−O bond cleavage TS2 is high (17.0 kcal/mol); however, the energy of the triplet product P2 is very close to the quintet P2 and is 4.5 kcal/mol. The final hydrogen abstraction from the O^3 is expected to be facile by analogy with the *transO*^{3}-O^{3}HO^5-L complex.

Summary of the O−O Bond Cleavage in the Protonated Acylperoxo Complexes. Importantly, both pathways I and II in the end produce [(Salen)Mn^V(O)L] and RCO$_2$H, regardless of the nature of the solvent and the axial ligand employed. This is in sharp contrast to the O−O bond cleavage in the trans acylperoxo complexes without the pull effect, where both reactive [(Salen)Mn^V(O)L] and unreactive [(Salen)Mn^{IV}(O)L] species could be formed.

The contribution from the two pathways for isomer *transO*^{3}-O^{3}HO^5-L depends on the relative activation energies of the quintet TS1 or TS1S and TS2. As seen from the Table 2 and Figure 3, the energies for the lowest TS1 and TS2 barriers with respect to the most thermodynamically stable *transO*^{5}-O^{3}HO^2-L complex are comparable and are 16.1 and 15.6 kcal/mol for L = NH$_3$ and 17.7 and 15.3 kcal/mol for L = HCO$_2^-$, respectively.

Note, however, that the barriers for *transO*^{3}-O^{3}HO^5-L isomer represent the upper bound for the O−O bond cleavage in the protonated complexes. For a special case of isomer *transO*^{3}-O^{3}HO^2-L, with L = NH$_3$ the TS2 barrier is further reduced to overall 13.3 kcal/mol. Furthermore, it is not unlikely that over the reaction course the unprotonated trans complex can be transformed directly into P1 bypassing the TS1 by protonation of Salen's O^2 oxygen from the solution, consequently reducing the overall barrier to 11.1 and 12.5 kcal/mol for L = NH$_3$ and HCO$_2^-$, respectively. While such possibility could dramatically enhance the O−O bond cleavage rate, it would still result in heterolysis of the O−O bond.

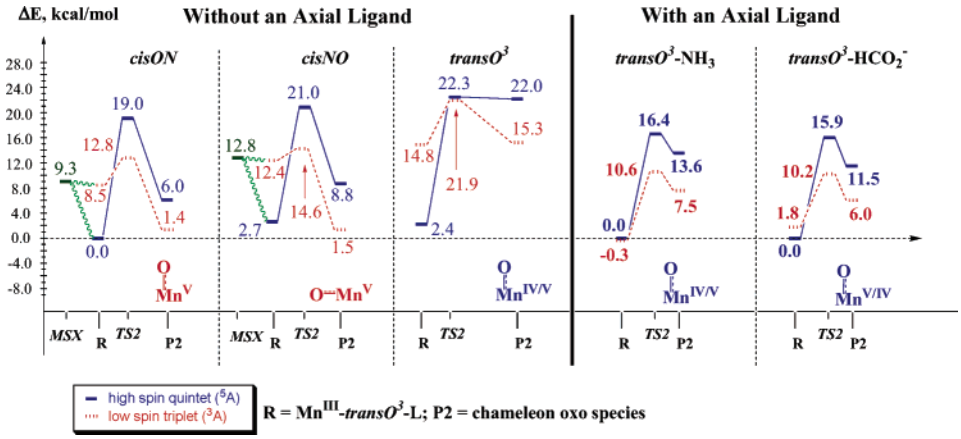

Figure 4. Cumulative energy diagram for the O−O bond cleavage in the unprotonated acylperoxo complexes. The solid lines connect the quintet profile, whereas dashed lines connect the triplet profile. The wavy lines represent spin-state transitions.

C. Chameleon Product P2: {[(Salen)Mn^{IV}(OH)L]-RCO$_2$} vs {[(Salen)Mn^{V}(OH)L]RCO$_2^-$}. The intermediates of the O−O bond cleavage in the above-discussed pathway II, *transO*^{3}-L P2, should be chameleon in nature and may be regarded as either radical pair {[(Salen)Mn^{IV}(OH)L]-RCO$_2$} or ion pair {[(Salen)Mn^{V}(OH)L]RCO$_2^-$}. The duality of the intermediate P2 is indicated in the analysis of Mulliken spin densities on the Mn, O^3, O^4, and O^5 atoms.

In the case of L = none, the spin densities of *transO*^{3}-O^{3}HO^5 P2 are 2.85, 0.07, 0.63, and 0.45, whereas those of *transO*^{3}-O^{3}HO^2 P2 are 3.01, 0.06, 0.87, and 0.00 for Mn, O^3, O^4, and O^5 atoms, respectively. These clearly suggest that both P2's comprise [(Salen)Mn^{IV}(OH)] and RCO$_2$ radical. In the case of *transO*^{3}-O^{3}HO^5, the RCO$_2$ radical attaches to the [(Salen)Mn^{IV}(OH)] complex through the O^3-H···O^5 hydrogen bond, whereas in the *transO*^{3}-O^{3}HO^2 complex the RCO$_2$ and [(Salen)Mn^{IV}(OH)] are connected by a weak O^3···O^4 interaction. Because of the difference in the interaction between the fragments, the unpaired electron of RCO$_2$ in *transO*^{3}-O^{3}HO^5 P2 is delocalized between the O^4 and O^5 atoms, whereas in the *transO*^{3}-O^{3}HO^2 P2 the unpaired electron is localized on O^4.

In the case of anionic axial ligand L = HCO$_2^-$, the spin densities in *transO*^{3}-O^{3}HO^5-L P2 are 2.78, 0.41, 0.57, and 0.00 on Mn, O^3, O^4, and O^5, respectively. Although the radical is coupled to the [(Salen)Mn^{IV}(OH)HCO$_2^-$] complex through O^3-H···O^5 hydrogen bond, the electron density on the RCO$_2$ radical is substantially reduced, whereas the spin density is substantially increased on O^3. This suggests that negatively charged axial ligand helps to develop more ionic character in P2, increasing the contribution from the [(Salen)-Mn^{V}(OH)L] and RCO$_2^-$ ion pair. Therefore, the nature of the P2 complex is indeed chameleon and depends on the electrostatic interaction between the fragments.

Further insights into the dual nature and importance of the electrostatic interactions appear from the computed relative energies of the heterolytic A1 and homolytic A2 dissociation asymptotes in the gas phase, toluene, and acetonitrile, shown in Table 2. The heterolytic asymptote A1 refers to infinitely separated ionic fragments [(Salen)-Mn^{V}(OH)L] and RCO$_2^-$, where the total charge on [(Salen)-Mn^{V}(OH)L] is the charge of L plus 2. For the homolytic asymptote A2, [(Salen)Mn^{IV}(OH)L] and RCO$_2$, the charge on the [(Salen)Mn^{IV}(OH)L] fragment is the charge of L plus 1. Note that the ground state of the free [(Salen)Mn^{V}(OH)L] species is a triplet. The corresponding quintet state is only 4.6, 0.7, and 0.2 kcal/mol higher than the triplet state for L = none, NH$_3$, and HCO$_2^-$, respectively, whereas the singlet states are substantially higher in energy. The ground state of [(Salen)Mn^{IV}(OH)L] is a quartet, with doublet states lying more than 17 kcal/mol higher.

Because the heterolytic asymptote implies substantial charge separation, its relative energy should strongly depend on the charge screening by the employed solvent. On the other hand, for the homolytic asymptote no charge separation occurs because the RCO$_2$ fragment is neutral and solvent effect should be less important. Indeed in the case of L = none, the energies of the heterolytic A1 and homolytic A2 asymptotes are 198.0 and 17.6 kcal/mol in the gas phase, 98.5 and 13.3 kcal/mol in toluene, and 29.5 and 10.3 kcal/mol in acetonitrile. Similarly, for L = NH$_3$ the A1 and A2 change from 182.8 and 11.0 kcal/mol in the gas phase to 81.7 and 5.5 kcal/mol in apolar toluene and finally to 9.5 and −0.1 kcal/mol in polar acetonitrile. When the charge of the [(Salen)Mn^{V}(OH)L] fragment is reduced, such as in the case L = HCO$_2^-$, the asymptotes A1 and A2 change from 111.2 and 6.9 kcal/mol to 44.9 and 4.0 kcal/mol in toluene and to 3.6 and 1.5 kcal/mol in acetonitrile. Because polar acetonitrile substantially stabilizes the heterolytic asymptote A1, the dual or chameleon nature of the intermediate P2 should be the most prominent in polar solvents.

D. Comparison of the Pull and Push Effects on the O−O Bond Cleavage. To highlight the influence of the pull effect on the mechanism and energetics of the O−O bond cleavage, we compare the results in the section B with the results of our previous work.[28,29,31] Figure 4 summarizes previous results on the pure O−O bond cleavage without and with the axial ligands but in the absence of the pull effect.[28,29,31] Note that in the Figure 4 we removed the paths for intramolecular oxidation of the catalyst's ligand into corresponding *N*-oxide because we do not discuss these pathways in the present paper.[28,29,31] Also we preserved the original labels in the Figure 4, noting however that original P2 is a close analogue of present P3/P4 products. Unlike in

the protonated complexes, only a single one-step pathway connects the acylperoxo complexes with the oxo species within a given spin state. Because the O−O bond breaking on the triplet surface has the lowest barrier, transitions from quintet to triplet spin state become important for complexes with a quintet ground state and large quintet−triplet energy gap. Axial ligands substantially reduce the quintet−triplet energy gap in the unprotonated *transO*^{3}-L complexes dropping the overall barriers to 10.9 and 10.6 kcal/mol for L = NH_3 and HCO_2^-, respectively. This is similar to the second reaction on the pathway I in the protonated acylperoxo complexes. However, in sharp contrast with the protonated complexes for the *transO*^{3}-L isomer, the final product *trans*-oxo species P2 are chameleon in nature.[28,29]

As we indicated in section B, several scenarios are possible for the O−O bond heterolysis in the protonated acylperoxo complexes, occurring within the range of the overall activation energies of 11.1−15.6 kcal/mol for L = NH_3 and 12.5−15.3 for L = HCO_2^- and possibly involving multiple spin transitions. Taking into account the expected error of the B3LYP method of 3−5 kcal/mol,[45] we cannot definitively state which O−O bond cleavage mechanism would be the most favorable. In the worst case the O−O bond cleavage under the pull effect would be kinetically less favorable than the O−O bond cleavage in the unprotonated complexes. There is also a possibility that the two mechanisms would have comparable reaction rates. In any case the ratio of the O−O bond cleavages in the protonated versus unprotonated complexes could be manipulated by changing the acidity of the system. As such in principle a selected mechanism can be shut off completely. The pull effect is beneficial because it introduces crucial qualitative change into the mechanism; it ensures heterolysis of the O−O bond. Consequently, the pull effect guarantees formation of the desired [(Salen)Mn^V(O)L] and prevents formation of unwanted [(Salen)Mn^{IV}(O)L] species. In practice, however, in acidic conditions the axial ligands may become protonated, forcing the O−O bond cleavage to proceed according to the case L = none mediated by cis acylperoxo complexes, and therefore, a careful choice of an axial ligand is critical.

Within the computational certainty we predict that the overall rate of the O−O bond cleavage should decrease due to the pull effect, increasing the ratio of the reactive Mn^V(O) species produced. We speculate that finding a way to disfavor formation of the thermodynamically more stable unreactive isomers will ultimately result in the clean and efficient heterolysis of the O−O bond of acylperoxo complexes under acidic conditions.

Finally, we note that the decrease in the O−O bond cleavage rate in the acidic conditions, as compared to basic conditions, is evidenced experimentally for analogous porphyrin Mn acylperoxo complexes in the case of electron-rich *p*-methylbenzoic peracid.[20] Also for Fe porphyrin catalyst it has been shown that the rate of decomposition of H_2O_2 is strongly reduced at low pH, concomitant with increase in the yield of the oxidation product.[22] This confirms that increasing acidity may be advantageous for the selectivity of oxidation.

IV. Conclusions

The conclusions from this study of the pull effect on the O−O bond cleavage in the KJK system are as follows:

A variety of cis and trans complexes of [(Salen)Mn^{III}(RCO$_3$H)L] and [(SalenH)Mn^{III}(RCO$_3$)L] have been identified computationally under acidic conditions. Protonation has been found to substantially increase the triplet−quintet energy gap in the acylperoxo complexes, securing the high-spin quintet ground state of the acylperoxo complexes. Interestingly, the unreactive *trans*-[(Salen)Mn^{III}(RCO$_3$H)L] complexes where peracid is coordinated to the metal via carbonyl oxygen are thermodynamically the most stable among the protonated complexes. Nevertheless, the O−O bond cleavage is possible in the less stable reactive isomers with peracids coordinated via peroxo oxygen. In contrast to the unprotonated complexes the O−O bond cleavage in the protonated complexes proceeds via two distinct multistep pathways. Most importantly, protonation brings an important qualitative change to the reaction mechanism—it ensures the O−O bond heterolysis, in sharp contrast to mixed homolysis/heterolysis in the unprotonated complexes. Thus, acidity provides means for regulating the mode of the O−O bond cleavage, allowing in principle to shut off the unwanted O−O bond homolysis of the unprotonated complexes completely. Although the pull effect ensures the O−O bond heterolysis and consequently formation of the desired [(Salen)Mn^V(O)L] species in acidic conditions, within certainty of the computational method and model system it may also retard the O−O bond cleavage rate. This finding is excellent agreement with experimental observations.[20,22]

Acknowledgment. This research is in part supported by a grant (CHE-0209660) from the National Science Foundation. Acknowledgment is made to the Cherry L. Emerson Center of Emory University for the use of its resources, which is in part supported by a National Science Foundation grant (CHE-0079627) and an IBM Shared University Research Award.

Supporting Information Available: Table 1S, a summary of important bond lengths for selected species, Table 2S, a summary of the spin densities for key optimized species, and Table 3S, Cartesian coordinates of all important structures optimized with B3LYP/LANL2DZ (in Å) along with energies and imaginary frequencies.

IC0490122

(45) Siegbahn, P. E. M.; Blomberg, M. R. A. *Chem. Rev.* **2000**, *100*, 421−437. Xu, X.; Kua, J.; Periana, R. A.; Goddard, W. A., III. *Organometallics* **2003**, *22*, 2057−2068.